New "USD" Hamiltonians for the *sd* shell

B. Alex Brown[1] and W. A. Richter[2]

[1]*Department of Physics and Astronomy, and National Superconducting Cyclotron Laboratory, Michigan State University, East Lansing, Michigan 48824-1321, USA*

[2]*Department of Physics, University of the Western Cape, Private Bag X17, Bellville 7530, South Africa*

(Received 23 May 2006; published 13 September 2006)

We derive new Hamiltonians for the *sd* shell, USDA and USDB, based on a renormalized G matrix with linear combinations of two-body matrix elements adjusted to fit a complete set of data for experimental binding energies and excitation energies for the *sd*-shell nuclei. These Hamiltonians provide a new level of precision for realistic *sd*-shell wave functions for applications to nuclear structure and nuclear astrophysics.

DOI: 10.1103/PhysRevC.74.034315 PACS number(s): 21.60.Cs, 21.10.Dr, 27.20.+n

I. INTRODUCTION

The USD Hamiltonian [1,2] has provided realistic *sd*-shell ($0d_{5/2}$, $0d_{3/2}$, $1s_{1/2}$) wave functions for use in nuclear structure models, nuclear spectroscopy, and nuclear astrophysics for over two decades. It is also an essential part of the Hamiltonian used for the *p-sd* [3] and *sd-pf* [4–6] model spaces. Results based on the USD Hamiltonian in 2005 include those in Refs. [7–32]. The USD Hamiltonian is defined by 63 *sd*-shell two-body matrix elements (TBME) and three single-particle energies (SPE) given in Table I of [1]. The values are derived from the renormalized G matrix with modifications needed to reproduce the experimental binding energies and excitation energies for nuclei in the region $A = 16$–40. In this paper we present results for new USD-type Hamiltonians called USDA and USDB based on an updated set of binding energies and energy levels.

Theoretical methods for calculating the effective TBME with a renormalized G matrix starting from NN interactions have evolved considerably [33]. However, there are several reasons why the renormalized G-matrix *sd*-shell (RGSD) TBME may not be accurate: (i) The perturbation expansion may not be converged [34]; (ii) the oscillator basis used for matrix elements and energy denominators is an approximation; and (iii) real three-body forces are required as observed for ab initio calculations of light nuclei [35]. Three-body forces contribute to the effective one- and two-body matrix elements when they are averaged over the nucleons in the closed core, ^{16}O in our case [36]. When applied to nuclei with three or more valence nucleons, both effective and real three-body interactions may play a role. Thus, to obtain realistic wave functions for medium-mass nuclei there is a need to modify the effective interactions based on constraints from experimental data. The resulting set of parameters for the effective interaction may be compared with the original G-matrix input to evaluate the contributions of higher order terms and three-body interactions.

The USD Hamiltonian was the culmination of about a decade of work to understand the energy levels and spectroscopic properties for *sd*-shell nuclei in terms of a "unified" Hamiltonian applied in the full *sd*-shell model space. The earliest applications of shell-model configuration mixing to the *sd*-shell were limited by computational power and had to be applied to truncations within the *sd*-shell space. For example, in 1968 Arima *et al*. [37] considered the properties of $A = 18$–20 in the model space of $[0d_{5/2}, 1s_{1/2}]^n$. The immediate predecessors to USD were the Chung-Wildenthal particle (CWP) and hole (CWH) Hamiltonians [38] that were obtained from fits to data in the lower and upper parts of the *sd* shell, respectively. As computational power advanced it became possible in the late 1970s to consider nuclei in the middle of the *sd* shell and eventually the CW Hamiltonians were merged into the "universal" *sd* (USD) Hamiltonian.

The original USD Hamiltonian was obtained from a least-squares fit of 380 energy data with experimental errors of 0.2 MeV or less (with most experimental errors being 10 keV or less) from 66 nuclei. The root-mean-square (rms) deviation between experimental and theoretical energies was about 150 keV (for 380 energy data with uncertainties of 200 keV or less). The number of states that were considered for each nucleus is shown in Fig. 1. The largest numbers of states are for those nuclei around $N = Z = 12$ and $N = Z = 17$. Although many energy levels were known in the middle of the shell, only a few were included in the USD fit owing to the computational limitations in the 1980s. Also, since 1980 there is much more and improved data for the neutron-rich nuclei. Today the computational effort is trivial—on a desktop PC it is possible to obtain a complete set of low-lying energy levels for all *sd*-shell nuclei in a few hours.

Thus we are motivated to refine the derivation of the USD Hamiltonian with an updated and complete set of energy data. We are able to consider 608 states in 77 nuclei distributed over *sd*-shell nuclei as shown in Fig. 2. The new Hamiltonians USDA and USDB lead to a new level of precision for realistic shell-model wave functions. In the next section we discuss experimental data. In Sec. III we review the linear-combination method for the least-squares fit. In Sec. IV we present the results for the new Hamiltonians, with results for binding energies and energy levels in Sec. V.

II. EXPERIMENTAL DATA

The data for the new fits was obtained from the most recent compilations. In the case of $A = 21$–40 nuclei most data for excited states are from the Supplement to Energy Levels of

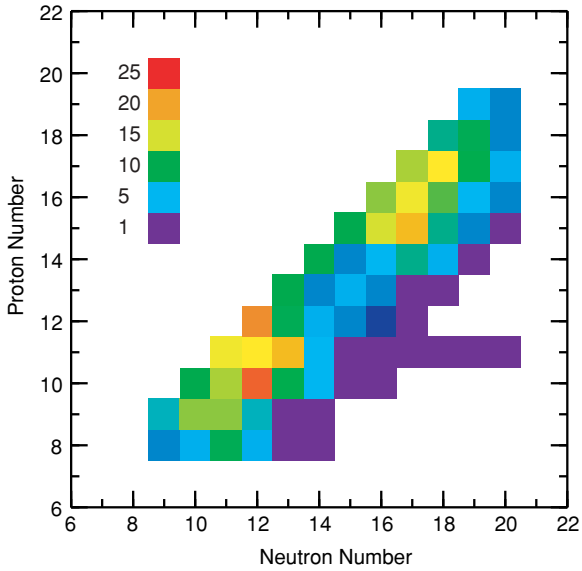

FIG. 1. (Color) Number of states used for the USD Hamiltonian for each nucleus.

$A = 21$–44 nuclei by P. M. Endt (published in 1998 [39]), used in conjunction with the previous complete review of nuclei in this mass range [40]. The supplement mainly discusses new data published in the period 1990–1996. A useful part of Endt's supplement is the inclusion of comparisons of positive-parity states with the USD predictions. More recent data are used for ^{20}O [32,41], ^{21}O [41], ^{23}O [42], ^{22}O [41],^{19}F, ^{20}F [43], ^{22}F [19,43], ^{23}F and ^{25}F [44], ^{27}F [45], ^{24}Ne [46], ^{27}Na [47], ^{28}Na and ^{29}Na [15], ^{24}Mg [48], and ^{33}Si [49].

The ground-state binding energies used are from the 2003 atomic mass evaluation of Audi, Wapstra, and Thibault [50]. These are supplemented with new results from [51] for ^{23}O, ^{23}F, ^{24}O, ^{25}F, ^{26}F, ^{27}F, ^{27}Ne, ^{28}Ne, ^{29}Ne, ^{30}Ne, ^{31}Na, and ^{32}Mg.

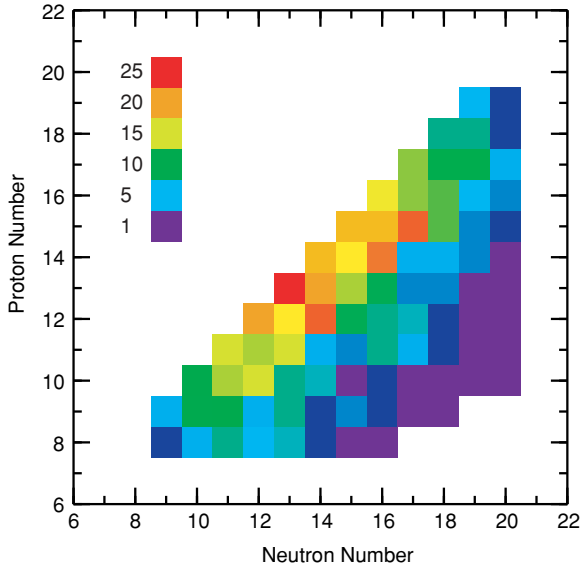

FIG. 2. (Color) Number of states used for the USDA and USDB Hamiltonians for each nucleus.

We take the binding energies relative to that of ^{16}O with the Coulomb energy correction used for USD [38],

$$BE(A,Z)^r = BE(A,Z) - BE(^{16}\mathrm{O}) - E_C(Z), \qquad (1)$$

with $E_C(Z) = 3.48$ ($Z = 9$), 7.45 ($Z = 10$), 11.73 ($Z = 11$), 16.47 ($Z = 12$), 21.48 ($Z = 13$), 26.78 ($Z = 14$), 32.47 ($Z = 15$), 38.46 ($Z = 16$), 44.74 ($Z = 17$), 51.31 ($Z = 18$), and 58.14 ($Z = 19$) MeV. The Coulomb energy corrections were obtained from energy differences of isobaric analog states for the nuclei near $N = Z$.

For the new Hamiltonian we consider 608 states in 77 nuclei. The distribution of these states over the *sd*-shell nuclei is shown in Fig. 2

Most of the new data have been added in the middle of the *sd* shell (where computations are now possible) and for neutron-rich nuclei. (We include in this figure the ground states for six nuclei in the "island of inversion" $N = 19$–20 and $Z = 10$–12, although as discussed in the following they are not included in the fit.)

III. FITTING PROCEDURE

The shell-model effective Hamiltonian can be written as a sum of one- and two-body operators (using similar notation to that used by Honma *et al.* [52] for the *pf* shell, which is based on the work of Chung and Wildenthal [1,38] for the *sd* shell):

$$H = \sum_a \epsilon_a \hat{n}_n + \sum_{a \leqslant b,c \leqslant d} \sum_{JT} V_{JT}(ab;cd)\hat{T}_{JT}(ab;cd), \qquad (2)$$

where $\hat{n}_a$ is the number operator for the spherical orbit a with quantum numbers (n_a, l_a, j_a) and

$$\hat{T}_{JT}(ab;cd) = \sum_{MT_z} A^\dagger_{JMTT_z}(ab) A_{JMTT_z}(cd) \qquad (3)$$

is the scalar two-body density operator for nucleon pairs in orbits a, b and c, d coupled to spin quantum numbers JM and isospin quantum numbers TT_z. We use a simplified notation

$$H = \sum_{i=1}^{p} x_i O_i, \qquad (4)$$

where the x_i stand for single-particle energies ϵ_a or the two-body matrix elements $V_{JT}(ab;cd)$, and the operators O_i stand for $\hat{n}$ or $\hat{T}$, respectively. The vector $\vec{x} = (x_1, x_2, \cdots, x_p)$ defines the Hamiltonian. This Hamiltonian will have eigenvectors ϕ_k and eigenvalues λ_k that can be expressed in terms of a linear combination of the Hamiltonian $\vec{x}$:

$$\lambda_k = \langle\phi_k|H|\phi_k\rangle = \sum_{i=1}^{p} x_i \langle\phi_k|O_i|\phi_k\rangle = \sum_{i=1}^{p} x_i \beta_i^k, \qquad (5)$$

where $\beta_i^k = \langle\phi_k|O_i|\phi_k\rangle$.

For a given starting Hamiltonian $\vec{x}^{\,s}$, we calculate β_i^k and then minimize the quantity

$$\chi^2 = \sum_{k=1}^{N} \left(\frac{E^k_{\mathrm{exp}} - \lambda_k}{\sigma^k_{\mathrm{exp}}} \right)^2, \qquad (6)$$

where $E^k_{\rm exp}$ are the experimental energies and $\sigma^k_{\rm exp}$ are the associated errors. This gives

$$\frac{\partial \chi^2}{\partial x_j} = \sum_{k=1}^{N} 2\frac{\left(E^k_{\rm exp} - \lambda_k\right)}{\left(\sigma^k_{\rm exp}\right)^2}\frac{\partial}{\partial x_j}\left(-\sum_{i=1}^{p} x_i \beta^k_i\right) = 0. \quad (7)$$

Without taking into account the implicit dependence of β^k_i on x_j through ϕ_i we obtain p linear equations for an improved Hamiltonian $\vec{x}$:

$$\sum_{k=1}^{N}\left(E^k_{\rm exp} - \sum_{i=1}^{p} x_i \beta^k_i\right)\frac{\beta^k_j}{\left(\sigma^k_{\rm exp}\right)^2} = e_j - \sum_{i=1}^{p}\gamma_{ij}x_i = 0, \quad (8)$$

where $j = 1, 2, \cdots, p$. This can be written in terms of a $p \times p$ matrix

$$G = (\gamma_{ij}) = \sum_{k=1}^{N}\frac{\beta^k_i \beta^k_j}{\left(\sigma^k_{\rm exp}\right)^2} \quad (9)$$

and a p-dimensional vector

$$\vec{e} = (e_i) = \sum_{k=1}^{N}\frac{E^k_{\rm exp}\beta^k_i}{\left(\sigma^k_{\rm exp}\right)^2} \quad (10)$$

as

$$G\vec{x} = \vec{e}. \quad (11)$$

Since G is a real symmetric matrix, it can be inverted to obtain the new Hamiltonian

$$\vec{x} = G^{-1}\vec{e}. \quad (12)$$

To take into account the implicit dependence of β^k_i on x_j this procedure is repeated (iterated) until convergence.

The matrix G^{-1} is referred to as the error matrix [53] since the diagonal elements are the square of the parameter errors and the off-diagonal matrix elements are related to the correlations between the parameters. As in most multiparameter fits, the resulting parameters x_i are highly correlated. In addition, the low-lying nuclear states are much more sensitive to some linear combinations of Hamiltonian parameters than others. These issues can be quantified by diagonalizing the matrix G :

$$D = AGA^T, \quad (13)$$

or in terms of the error matrix,

$$D^{-1} = AG^{-1}A^T, \quad (14)$$

where D is a p-dimensional diagonal matrix with positive elements D_i. The eigenvalues of the error matrix D^{-1} are $d_i = 1/D_i$. With this definition for A, Eq. (11) is equivalent to $D\vec{y} = \vec{c}$, where $\vec{y} = A\vec{x}$ and $\vec{c} = A\vec{e}$, which has the simple solution

$$y_i = c_i d_i. \quad (15)$$

The least-squares fit is thus reformulated in terms of uncorrelated linear combinations. The orthogonal parameters y_i are linear combinations of the Hamiltonian parameters x_i, with associated errors d_i. It is clear from Eq. (15) that, for large d_i, the values of y_i are strongly affected by a small change in the data c_i. Therefore, such linear combinations are only poorly determined by a given set of data. We can separate poorly determined linear combinations from well-determined ones by setting a certain criterion on the magnitude of the corresponding eigenvalues d_i.

The fitting procedure can be modified as follows. We start with the best available Hamiltonian $\vec{x}^{\,s}$. From the fit, mutually independent linear combinations y_i are determined according to Eq. (15). At the same time linear combinations of the starting Hamiltonian $\vec{x}^{\,s}$ are also obtained from $\vec{y}^{\,s} = A\vec{x}^{\,s}$. Then new linear combinations $\vec{y}^{\,a}$ are defined by adopting only well-determined values of y_i and using the starting values for the rest,

$$y^a_i = y_i(d_i \leqslant \delta) + y^s_i(d_i > \delta), \quad (16)$$

where δ is taken to be a suitable value for the criterion. The number of well-determined linear combinations is denoted by N_d. A new Hamiltonian is obtained from $\vec{x}^{\,a} = A^{-1}\vec{y}^{\,a}$, which is used for the next iteration to obtain $\vec{x}^{\,b} = A^{-1}\vec{y}^{\,b}$ from

$$y^b_i = y_i(d_i \leqslant \delta) + y^s_i(d_i > \delta). \quad (17)$$

This procedure is iterated until convergence.

This linear-combination (LC) method for finding the well-determined uncorrelated linear combinations of Hamiltonian parameters was used by Arima *et al.* [37] for the $d_{5/2}$-$s_{1/2}$ model space and by Macfarlane for the p shell [54]. The LC method together with the iteration method was used by Chung and Wildenthal to determine the original USD Hamiltonian [1,38], which was the starting point of the present work. The LC method was used in the pf shell to obtain the FPMI3 [55] and GXFP [52,56] Hamiltonians. More recently, it has been used in for the ($f_{5/2}$, $p_{3/2}$, $p_{1/2}$, $g_{9/2}$) model-space description of the Ni isotopes and $N = 50$ isotones [57].

IV. RESULTS FOR THE FIT

The calculations for the wave functions, energies, occupation numbers, and scalar two-body transition densities were carried out with OXBASH [58]. One iteration took about 12 hours on a desktop PC.

For the data set we consider all ground-state binding energies and all positive-parity energy levels for *sd*-shell nuclei. The first criterion for inclusion of the nth J^π level in the fit is whether or not the J^π for all lower states are known. Generally this means that we cannot consider states above the energy where one level has an unknown J^π. This usually occurs starting at $E_x = 5$–7 MeV. The second criterion is the energy at which the experimental level density for a given J^π becomes suddenly higher than the theoretical level density. This is a signature of intruder states. There is a well-defined region of nuclei with $N = 19 - 20$ and $Z = 10 - 12$ where the difference between the experimental and theoretical ground-state binding energies is much larger than the rms average. These nuclei are in the island of inversion that requires the explicit extension of the pf-shell orbits to the model space [4]. Ground and excited states for these six nuclei are not included in the fit. In the end we will show the comparison of all experimental levels to all theoretical levels.

With this selection we are able to consider 608 states in 77 nuclei with errors of less than 0.2 MeV (with most experimental errors being 10 keV or less). The uncertainty used in Eq. (6) is the experimental uncertainty $\sigma_{\rm exp}$ folded

quadratically with a theoretical error that is close to the rms value obtained in the best fit for which we take $\sigma_{\rm th} = 0.1$ MeV:

$$(\sigma^k)^2 = \left(\sigma^k_{\rm exp}\right)^2 + \left(\sigma^k_{\rm th}\right)^2. \quad (18)$$

We include ground-state binding energies in the fit directly in terms of their calculated E and β values. Excited states are included in the fit by taking the differences $E - E_{\rm gs}$ and $\beta - \beta_{\rm gs}$. This allows for states in exotic nuclei to be included where the $E - E_{\rm gs}$ is known more accurately (for example, from γ-ray transitions) than $E_{\rm gs}$.

As was done for USD, the SPE are taken to be constant (mass independent). One could add some mass dependence to the SPE, but it has little effect on the rms since it can be compensated by a change in the TBME (in particular in the monopole TBME combinations).

One can define the "effective SPE" by the addition of the monopole linear combinations of the TBME [59] to the original SPE. The effective SPE are well defined by the data, but the division into their separate SPE and monopole TBME parts cannot be made on the basis of *sd*-shell data (i.e., it must come from a theoretical model).

As was done for USD, we employ a mass dependence of the two-body matrix elements of the form

$$V_{JT}(ab;cd)(A) = \left(\frac{18}{A}\right)^p V_{JT}(ab;cd)(A = 18), \quad (19)$$

with $p = 0.3$. This accounts qualitatively for the mass dependence expected from the evaluation of a medium-range interaction with harmonic-oscillator radial wave functions. With $\hbar\omega = 41A^{-1/3}$, the matrix elements for a delta-function interaction scale analytically as $A^{1/2}$ and the matrix elements of the Coulomb interaction scale analytically as $A^{1/6}$. The rms of the fit has a shallow minimum near $p = 0.3$. The minimum is shallow because the mass dependence can be partly compensated by a change in the fitted values of the TBME.

The poorly determined linear combinations of Hamiltonian parameters were always constrained to the values obtained from the renormalized G matrix applied to the *sd* shell (RGSD). The calculations were based on the Bonn-A NN potential and include diagrams up to third order as well as folded diagrams. The TBME are given in Table 20 of [33].

For the present work the original USD Hamiltonian was used for the first iteration. Then the equations were iterated with $N_d = 30$ well-determined (varied) linear combinations with the remaining 36 poorly determined linear combinations set to the RGSD values. This was continued until the energies and $\vec{x}$ values converged to the level of about 10 keV. This rather highly constrained Hamiltonian is called USDA. In Fig. 3 we show the eigenvalues D_i of the fit matrix for USDA. A physically interesting quantity from the fit is the rms deviation between experimental and theoretical energies,

$$\text{rms} = \sqrt{\frac{1}{N}\sum_{k=1}^{N}\left(E^k_{\rm exp} - E^k_{\rm th}\right)^2}. \quad (20)$$

In Fig. 4 we show this rms deviation (solid line) as a function of the number of varied linear combinations N_d obtained for the final iteration of USDA (with the actual USDA corresponding to the results obtained at $N_d = 30$). The individual contributions to Eq. (20) are shown in Fig. 5 The rms deviation of the fitted and RGSD two-body matrix elements as a function of N_d are shown by the points connected by a dashed line in Fig. 4

TABLE I. Comparison of *sd* shell TBME for $T = 1$ (in MeV). $v(a, b, c, d; JT) = V_{JT}(ab; cd)(A = 18)$. The orbits are labeled by $1 = s_{1/2}$, $3 = d_{3/2}$, and $5 = d_{5/2}$.

Matrix element	USD	RGSD	USDA	USDB
v(5 5 5 5; 0 1)	−2.8197	−2.5418	−2.4796	−2.5598
v(5 5 3 3; 0 1)	−3.1865	−2.9807	−3.5693	−3.1025
v(5 5 1 1; 0 1)	−1.3247	−1.0885	−1.1572	−1.5602
v(3 3 3 3; 0 1)	−2.1845	−1.1624	−1.5050	−1.8992
v(3 3 1 1; 0 1)	−1.0835	−0.7911	−0.9834	−1.0150
v(1 1 1 1; 0 1)	−2.1246	−2.0617	−1.8461	−1.6913
v(5 3 5 3; 1 1)	1.0334	−0.4249	0.2510	0.6556
v(5 3 3 1; 1 1)	0.1874	−0.0304	0.0736	−0.0456
v(3 1 3 1; 1 1)	0.6066	0.3994	0.3105	0.5158
v(5 5 5 5; 2 1)	−1.0020	−0.9932	−0.9899	−1.0007
v(5 5 5 3; 2 1)	−0.2832	−0.1394	−0.3092	−0.2137
v(5 5 5 1; 2 1)	−0.8616	−0.7957	−0.7746	−0.9317
v(5 5 3 3; 2 1)	−1.6221	−0.9399	−1.1335	−1.2187
v(5 5 3 1; 2 1)	0.6198	0.8477	0.8901	0.8866
v(5 3 5 3; 2 1)	−0.3248	−0.4043	0.2248	−0.1545
v(5 3 5 1; 2 1)	−0.4770	−0.2469	0.1022	−0.3147
v(5 3 3 3; 2 1)	−0.6149	−0.9871	−0.5208	−0.5032
v(5 3 3 1; 2 1)	0.5247	0.6449	0.2811	0.3713
v(5 1 5 1; 2 1)	−0.8183	−1.2335	−0.9039	−0.9405
v(5 1 3 3; 2 1)	−0.4041	−0.6317	−0.5542	−0.3173
v(5 1 3 1; 2 1)	1.9410	1.4633	1.7072	1.6131
v(3 3 3 3; 2 1)	−0.0665	0.1427	−0.1570	−0.0974
v(3 3 3 1; 2 1)	0.5154	0.1787	0.1368	0.3494
v(3 1 3 1; 2 1)	−0.4064	−0.2767	−0.2533	−0.3034
v(5 3 5 3; 3 1)	0.5894	0.5050	0.4777	0.7673
v(5 3 5 1; 3 1)	−0.6741	−0.1021	−0.4507	−0.5525
v(5 1 5 1; 3 1)	0.7626	0.2781	0.6470	0.6841
v(5 5 5 5; 4 1)	−0.1641	0.0356	−0.2136	−0.2069
v(5 5 5 3; 4 1)	−1.2363	−1.4942	−1.3155	−1.3349
v(5 3 5 3; 4 1)	−1.4474	−1.6941	−1.2509	−1.4447

The motivation for 30 linear combinations can be seen in Fig. 4 One observes a plateau in the rms energy deviation of about 170 keV between 30 and 45 linear combinations. Beyond this there is a gradual drop until about 56 linear combinations with an rms deviation of 130 keV that does not significantly decrease going out to the full set of 66 combinations. Thus we also derive another Hamiltonian called USDB by varying 56 linear combinations of parameters. Three more iterations were required for convergence. As seen in the histogram in the upper right-hand corners of Figs. 5 and 6 the scatter between experiment and theory for USDB is systematically reduced compared to that for USDA. We include in Figs. 5 and 6 six data points not included in the fit—those for the ground states of ^{29,30}Ne, ^{30,31}Na, and ^{31,32}Mg—to show the large deviation for these nuclei in the island of inversion. The TBME for $A = 18$ are given in Tables I and II for $T = 1$ and $T = 0$, respectively. The TBME for other A values are given by Eq. (19). The single-

TABLE II. Comparison of *sd* shell TBME for $T = 0$ (in MeV). $v(a, b, c, d; JT) = V_{JT}(ab; cd)(A = 18)$. The orbits are labeled by $1 = s_{1/2}$, $3 = d_{3/2}$, and $5 = d_{5/2}$.

Matrix element	USD	RGSD	USDA	USDB
v(5 5 5 5; 1 0)	−1.6321	−1.4315	−1.4277	−1.3796
v(5 5 5 3; 1 0)	2.5435	3.1790	3.0520	3.4987
v(5 5 3 3; 1 0)	0.7221	1.7666	1.9658	1.6647
v(5 5 3 1; 1 0)	1.1026	0.3628	0.3967	0.0272
v(5 5 1 1; 1 0)	−1.1756	−0.8749	−0.8900	−0.5344
v(5 3 5 3; 1 0)	−6.5058	−6.5104	−6.5106	−6.0099
v(5 3 3 3; 1 0)	0.5647	−0.0200	0.0136	0.1922
v(5 3 3 1; 1 0)	1.7080	1.7250	1.5511	1.6231
v(5 3 1 1; 1 0)	2.1042	1.8887	1.9021	2.0226
v(3 3 3 3; 1 0)	−1.4151	−1.3404	−1.4927	−1.6582
v(3 3 3 1; 1 0)	−0.3983	−0.8402	−1.0014	−0.8493
v(3 3 1 1; 1 0)	0.0275	0.0405	0.0949	0.1574
v(3 1 3 1; 1 0)	−4.2928	−3.3056	−3.8051	−4.0460
v(3 1 1 1; 1 0)	−1.2501	−0.2441	−0.6655	−0.9201
v(1 1 1 1; 1 0)	−3.2628	−3.3313	−3.8693	−3.7093
v(5 3 5 3; 2 0)	−3.8253	−4.5004	−4.5452	−4.2117
v(5 3 5 1; 2 0)	−0.0968	−1.2555	−1.0254	−0.6464
v(5 3 3 1; 2 0)	0.2832	−1.4793	−1.2803	−0.4429
v(5 1 5 1; 2 0)	−1.4474	−0.4109	−0.4874	−0.3154
v(5 1 3 1; 2 0)	−2.0664	−2.7050	−2.5947	−2.5110
v(3 1 3 1; 2 0)	−1.8194	−1.3883	−1.7530	−1.8504
v(5 5 5 5; 3 0)	−1.5012	−0.8478	−1.4018	−1.6651
v(5 5 5 3; 3 0)	2.2216	2.1769	2.2427	2.3102
v(5 5 5 1; 3 0)	−1.2420	−1.4992	−1.7954	−1.2167
v(5 5 3 3; 3 0)	1.8949	0.8466	0.9812	1.1792
v(5 3 5 3; 3 0)	−0.5377	−1.0712	−1.2963	−1.2124
v(5 3 5 1; 3 0)	1.2032	1.0367	0.8962	1.2526
v(5 3 3 3; 3 0)	2.0337	2.1625	1.8985	1.4300
v(5 1 5 1; 3 0)	−3.8598	−3.6000	−3.9337	−4.1823
v(5 1 3 3; 3 0)	0.1887	0.1668	0.4599	0.0968
v(3 3 3 3; 3 0)	−2.8842	−2.9026	−2.9800	−2.9660
v(5 3 5 3; 4 0)	−4.5062	−4.4330	−4.4652	−4.6189
v(5 5 5 5; 5 0)	−4.2256	−3.6858	−4.3811	−4.3205

particle energies for ($d_{5/2}$, $s_{1/2}$, $d_{3/2}$) are (−3.9478, −3.1636, 1.6466) MeV for USD, (−3.9436, −3.0612, 1.9798) MeV for USDA, and (−3.9257, −3.2079, 2.1117) MeV for USDB.

The fitted and input RGSD (G matrix) TBME are shown in Fig. 7. The USDA TBME are similar to the RGSD with an rms deviation between the TBME of 290 keV (see Fig. 4). Compared to the maximum magnitude of 6 MeV for the TBME, this represents only a 5% rms difference. However, this specific 5% change is critical for obtaining accurate binding energies and spectra. The USDB Hamiltonian, where 56 parameters are varied, is compared with RGSD in middle panel of Fig. 7; the result is a 375-keV rms difference for the TBME (6% of the largest). When the rms sum in Eq. (20) is restricted to the original set of energy data used for the original USD interaction (380 data points with σ^k of 200 keV or less) the result is 171 and 126 keV for USDA and USDB, respectively. Thus the added data do not worsen the quality of the fit, but they do provide more constraints on the determination of the TBME.

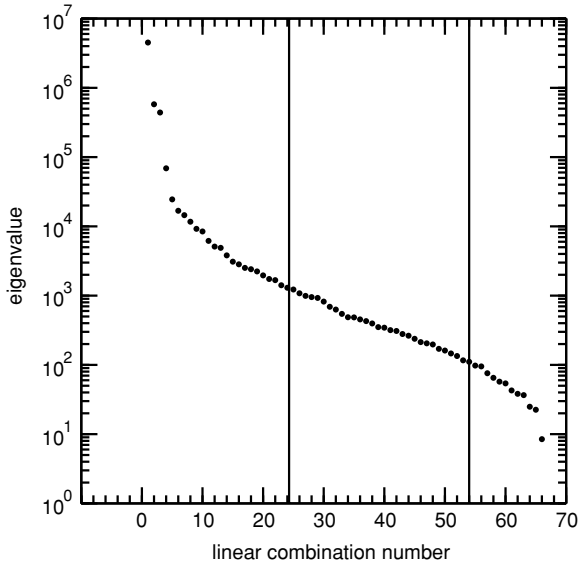

FIG. 3. Eigenvalues D_i of the fit matrix.

Thus we have two new Hamiltonians: a conservative one, USDA, which is closest to RGSD and gives a good but not the best fit to the data, and another, USDB, that differs more from RGSD but gives a best fit to the data. Calculation of other observables such as spectroscopic factors, moments, and γ- and β-decay rates with both USDA and USDB will give an estimate of the theoretical errors attributable to the *sd*-shell Hamiltonian as well as determine whether or not USDB is in fact superior to USDA. The original USD and RGSD TBME are compared on the right-hand side of Fig. 7. USD deviates the most from RGSD with a 450-keV rms in the TBME perhaps because of the smaller data set used for its determination.

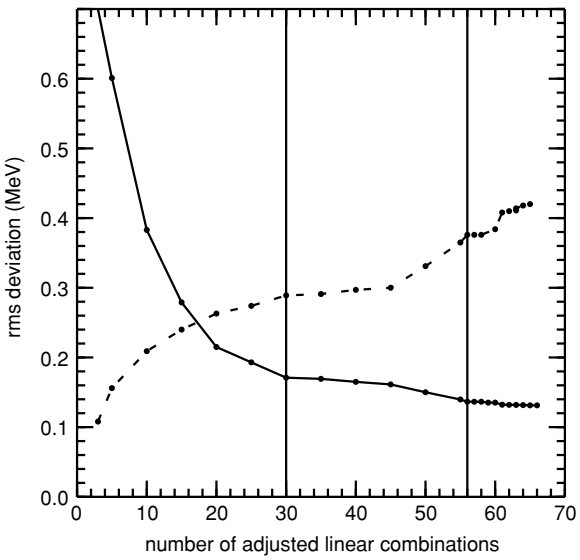

FIG. 4. The rms deviations as a function of the number of fitted linear combinations for the final USDA iteration. The points connected by a line show the deviation between experimental and theoretical *sd*-shell energies. The points connected by a dashed line show the rms deviation between the two-body matrix elements for the USD and RGSD Hamiltonians.

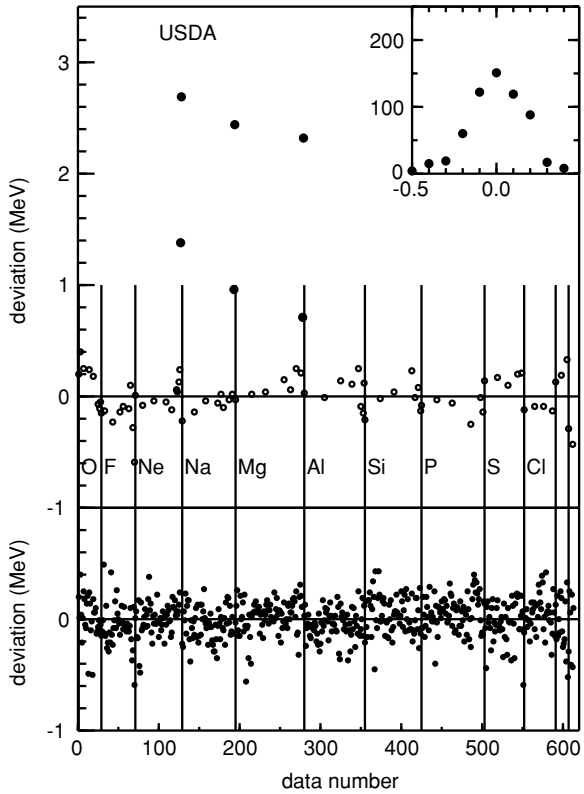

FIG. 5. Deviations between experimental and theoretical energies for USDA. The ground-state binding energies are plotted on the top panel and the excitation energies on the bottom. The inset shows a histogram of the deviations binned over 100-keV intervals.

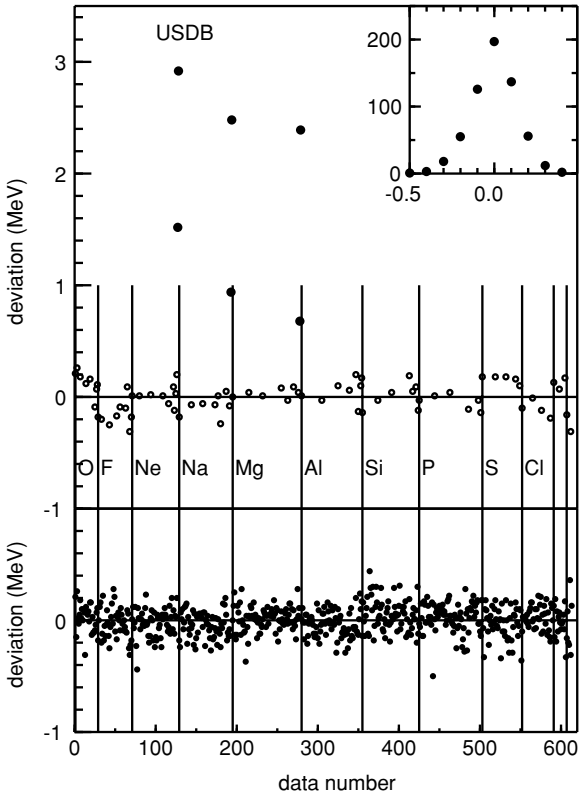

FIG. 6. Same as Fig. 5 except for the USDB Hamiltonian.

The monopole linear combinations of TBME are among the most important for the fit:

$$\bar{V}_{ab,T} = \frac{\sum_J (2J+1) V_{JT}(ab;ab)}{\sum_J (2J+1)}. \quad (21)$$

They combine with the SPE to determine how the effective SPE evolve as a function of N and Z. The monopole combinations for the various interactions are compared in Fig. 8. The values for USDA and USDB are essentially the same. They are also close to the original USD except for the $s_{1/2}$-$s_{1/2}$ and $d_{5/2}$-$d_{3/2}T = 0$ terms being 500 keV smaller for USD.

The $T = 0$ monopole terms are large and attractive with a general agreement between USD and RGSD in the overall pattern. The $d_{5/2}$-$d_{3/2}T = 0$ monopole term is the largest. This term with its large tensor interaction component is responsible for the change in shell structure as a function of N and Z in the *sd* shell [60]. This strong tensor contribution is important for the changes in shell structure for all nuclei [60,61]. All of the USD Hamiltonians deviate from the RGSD values by as much as 1 MeV for both $T = 0$ and $T = 1$.

For USDB the $A = 17$ single-particle energies are -3.93, -3.21, and 2.11 MeV for $d_{5/2}$, $s_{1/2}$, and $d_{3/2}$, respectively, to be compared with experimental values of -4.14 and -3.27 for $d_{5/2}$ and $s_{1/2}$. The $d_{3/2}$ particle strength in ^{17}O lies above the neutron-decay threshold and can only be observed in particle-transfer reactions. The ^{16}O$(d, p)^{17}$O reaction has only been analyzed [62] for the lowest and strongest $3/2^+$ state at 5.08 MeV corresponding to a $d_{3/2}$ SPE of $5.08 - 4.14 = 0.94$ MeV. There are states seen at higher energy in these reactions that have not been analyzed that could contain fragmented $d_{3/2}$ strength, and the spectra above 7 MeV were not measured. Thus the position of the centroid $d_{3/2}$ strength in ^{17}O is not known.

For USDB the $A = 39$ single-hole energies, $-[BE(^{40}\text{Ca}) - BE(^{39}\text{Ca})]$, are -15.47, -18.11, and -23.41 MeV for $d_{3/2}$, $s_{1/2}$, and $d_{5/2}$ respectively, to be compared with experimental values of -15.64 and -18.11 for $d_{3/2}$ and $s_{1/2}$. The $d_{5/2}$ particle strength in ^{39}K is fragmented over many states in the energy range of 4.5–10 MeV [63] with a centroid value of about 7.5 MeV corresponding to a neutron-hole SPE of $-15.64 - 7.5 = -23.1$ MeV. Experiment and calculation are in good agreement.

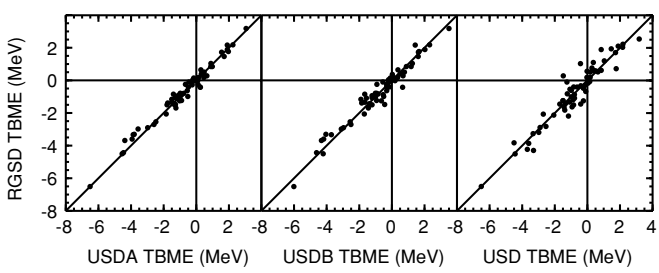

FIG. 7. Comparison of the fitted and RGSD TBME.

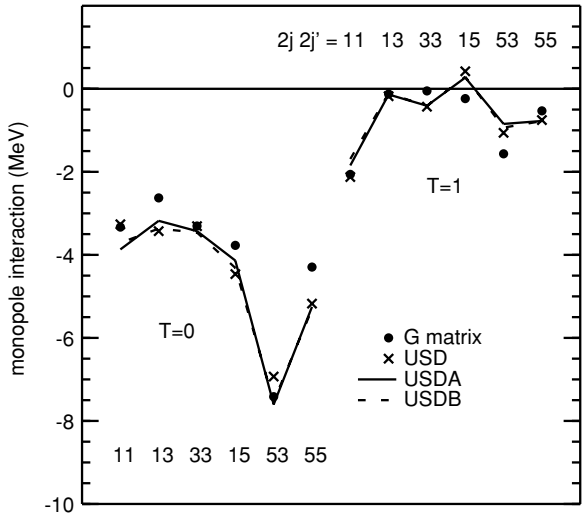

FIG. 8. The *sd*-shell monopole interactions. The solid lines are for USDA and USDB, the crosses are for USD, and filled circles for the RGSD.

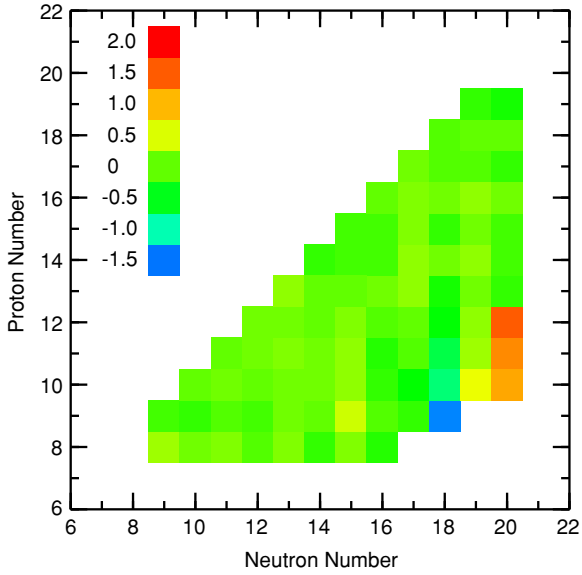

FIG. 9. (Color) Difference between the experimental and theoretical (USD) ground-state binding energies. A positive value indicates that experiment is more bound than theory.

The USDB neutron-hole SPE for ^{28}O (an unbound nucleus) are 0.17, −4.64, and −7.45 MeV for $d_{3/2}$, $s_{1/2}$, and $d_{5/2}$, respectively. The positive value for the highest hole state gives the marginally unbound nature of $^{25-28}$O. Note that the spin-orbit splitting is still large in this very neutron-rich nucleus. Also note the large SPE gaps for both $d_{3/2}$-$s_{1/2}$ and $d_{1/2}$-$d_{5/2}$ that are related to the observed shell gaps in the doubly-magic nuclei ^{24}O and ^{22}O, respectively [64].

The USD proton particle SPE for ^{28}O $[BE(^{29}\mathrm{F}) - BE(^{28}\mathrm{O})]$ are −19.90, −16.40, and −12.99 MeV for $d_{5/2}$, $s_{1/2}$, and $d_{3/2}$, respectively (which includes the Coulomb correction of 3.48 MeV). The protons are of course deeply bound in ^{28}O. The stability of ^{29}F is determined by the neutron separation energy. With USDB, ^{29}F is 0.8 MeV more bound than ^{28}F, in agreement with its observed stability. The experimental binding energy difference is 1.0 ± 0.8 MeV. (The large error in ^{28}F and ^{29}F precludes them from having any influence in the fit and it is not clear whether these nuclei are in the island of inversion.)

V. RESULTS FOR BINDING ENERGIES AND SPECTRA

For the binding energies, it is instructive to compare the results of the original USD with the updated set of data as shown in Fig. 9. Most of the differences lie in the nominal rms range of 150 keV. The binding energies predicted for the neutron-rich fluorine ($Z = 9$) isotopes turn out to be larger than experiment by up to 1.5 MeV. This indicates that the USD TBME involving the $d_{3/2}$ orbital in this mass region are incorrect. The oxygen isotopes ($Z = 8$) beyond $N = 16$ are known to be unbound [65–70] and the neutron-decay properties are not yet measured. The USD predicts that these nuclei are unbound except for ^{26}O, which is bound by 1.0 MeV with USD. Thus both neutron-rich oxygen and fluorine are too tightly bound with USD. In contrast, the binding energies predicted for $Z = 10$–12 and $N = 20$ are larger than experiment by up to 1.5 MeV. This indicates that the USD TBME are incorrect or that other shell-model configurations dominate the wave functions.

The binding energy difference for USDB is shown in Fig. 10 (The results for USDA are similar.) The fluorine problem for USD is corrected by the new USDA and USDB Hamiltonians. In addition, all of the oxygen isotopes are unbound with USDA and USDB. However, the $Z = 10 - 12$, $N = 20$ difference cannot be corrected, confirming the intruder state (island-of-inversion) interpretation for these nuclei. Although ^{28,29}F appear to lie outside of the island of inversion, they

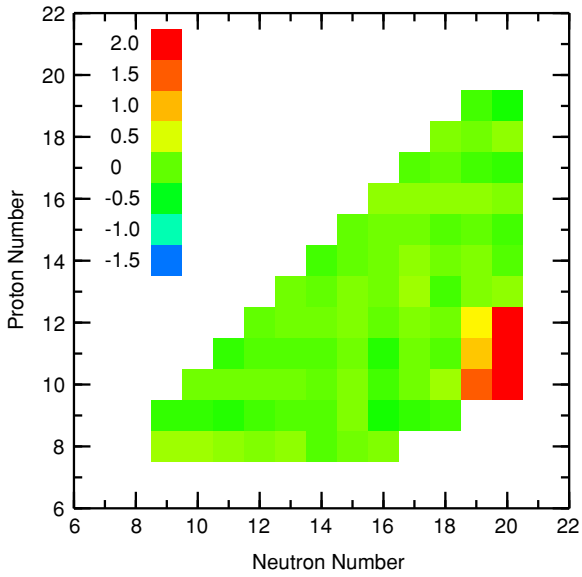

FIG. 10. (Color) Difference between the experimental and theoretical (USDB) ground-state binding energies. A positive value indicates that experiment is more bound than theory.

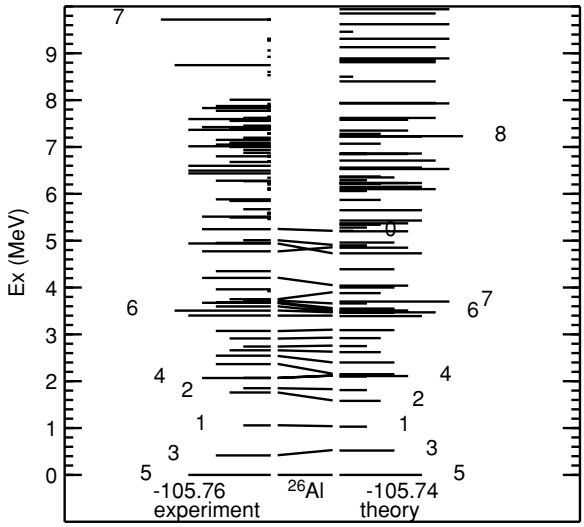

FIG. 11. Comparison of experimental and USDB theoretical levels ($T = 0$) for ^{26}Al. See the text for details.

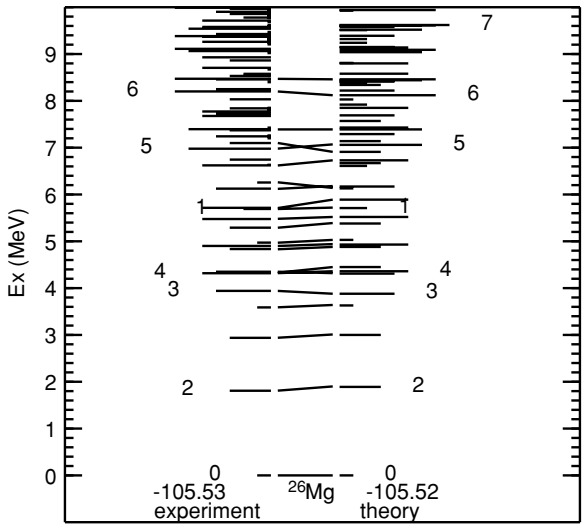

FIG. 12. Comparison of experimental and USDB theoretical levels for ^{26}Mg. See the text for details.

have large experimental errors (0.5–0.6 MeV) and they were thus not included in the fit. The improved USDA and USDB results for the ground-state binding energies of the neutron-rich fluorine and oxygen isotopes with $N \geqslant 16$ are related to the increased energy for the effective $d_{3/2}$ SPE. We note that this particular problem with USD was corrected when it was applied to the sd-pf model space [5].

Spectra were calculated for all 87 sd-shell nuclei for both USDA and USDB and compared to experiment. The compete set of comparisons can be found on the Web [71]. As an example, we show the results for $A = 26$. The spectrum for the positive-parity states in ^{26}Al with $T = 0$ is shown in Fig. 11. Experiment is shown on the left-hand side with lines that indicate the J value for the known positive-parity states. The lowest J value is labeled. Levels with an unknown J^π assignment are shown by the shortest lines, with the first such level for ^{26}Al lying at about 4 MeV. The theoretical levels are shown on the right-hand side, also indicated by lines of different length for the J value. The experimental and theoretical levels joined by a line in the middle are those included in the fit. The slope of these lines shows the difference between experiment and theory for the excitation energy. The ground-state binding energies are shown at the bottom. Starting at about 4 MeV we cannot make a level to level assignment between theory and experiment owing to the incomplete experimental information. From 4–6 MeV the experimental and theoretical level densities are similar; but there are too many levels of unknown spin-parity to make definitive associations between experiment and theory.

Above 6 MeV in ^{26}Al the experimental level density becomes higher, indicating the onset of intruder states (e.g., wave functions that contain the excitation of two or more nucleons out of the $0p$ shell or into the $1p0f$ shell). Generally toward the beginning and end of the sd shell where the sd-shell level density is smaller, the intruder states are more obvious in the low-lying spectra. For example, in ^{18}O two 0^+ states appear below 6 MeV compared to only one in the theory. The structure of this extra 0^+ in terms of p-shell excitations is well known [72]. In the upper part of the sd shell we find for example the lowest 2^+ state in ^{34}Si experimentally at 3.2 MeV and theoretically at 5.2 MeV. The lowest 2^+ state is interpreted as the neutron $2p$-$2h$ configuration that becomes the ground state in the island-of-inversion nuclei ^{32}Mg and ^{30}Ne [5].

The spectrum for ^{26}Mg (shown in Fig. 12) is another nucleus for which there is much well-established experimental data. All positive-parity levels are well matched between experiment and theory up to 6.5 MeV. Above this point there are levels with unknown spin and only a few high-spin levels can be matched. Above about 7.5 MeV the experimental level density becomes higher than that of theory.

For ^{26}Na (shown in Fig. 13) there are few experimental data with spin assignments to compare to theory. Recent results for ^{26}Na have been obtained from the ^{14}C(^{14}C, d)

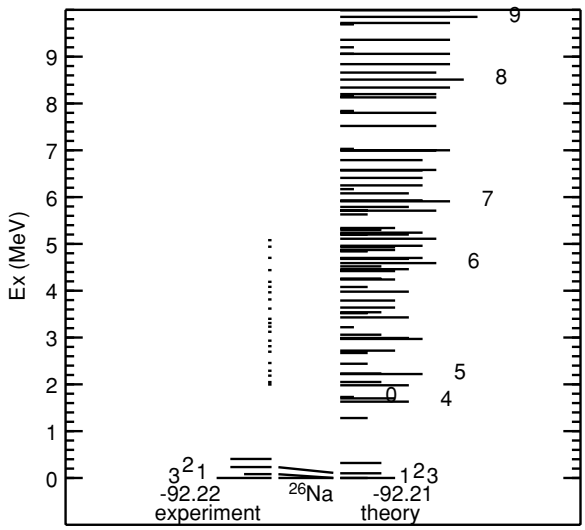

FIG. 13. Comparison of experimental and USDB theoretical levels for ^{26}Na. The theoretical ground state is 3^+ with the first excited 1^+ at 4 keV. See the text for details.

TABLE III. Gamow-Teller (GT) β-decay properties for ^{26}Ne (0^+) $\rightarrow$ ^{26}Na (1^+). The B(GT) values include an overall quenching factor of 0.6 [76].

Experiment		USD		USDA		USDB	
E_x (MeV)	B(GT)	E_x (MeV)	B(GT)	E_x (MeV)	B(GT)	E_x (MeV)	B(GT)
0.083	0.52(1)	0	0.61	0.077	0.51	0.004	0.46
1.511	0.07(1)	1.531	0.08	1.409	0.11	1.281	0.17
2.723	0.12(2)	2.271	0.14	2.412	0.11	2.450	0.14
		2.720	0.074	2.600	0.003	2.677	0.008

reaction [73]. The low-lying quadruplet is now established with the fourth state being 2^+, in agreement with theory. In the region 1–3 MeV 14 levels are predicted and 14 levels are seen in experiment, but still most levels do not have an experimental spin assignment. The highest spin of 5^+ predicted at 2.25 MeV is seen at 2.28 MeV in experiment. The 1^+ states can be assigned from the β decay of ^{26}Ne; the results are shown in Table III. It was noted [73,74] that the USD Hamiltonian predicted that four 1^+ states should be seen in the β decay of ^{26}Ne [75], but only three were observed in experiment [74]. The USDA and USDB results in Table III show that the fourth 1^+ state has a very small B(GT) value (much smaller than the USD value), indicating that it would be too weak to be observed. As noted in [73] several levels in the region of 3 MeV have γ-decay properties consistent with spin-parity 1^+. A future project will be to apply the new Hamiltonians to the γ-decay properties of ^{26}Na as well as other *sd*-shell nuclei. (The 1^+ states from [74] were not included in the fit owing to the disagreement in the number of 1^+ states that should be observed.)

For ^{26}Ne (shown in Fig. 14) there are little experimental data. The ground-state and first excited 2^+ state energies are in good agreement with theory. The 0^+ state found in experiment at 3.69 MeV is significantly lower than the theoretical state at 4.39 (4.63) MeV with USDA (USDB), indicating that this is an intruder state perhaps associated with the $(sd)^{n-2}(pf)^2$ configuration that becomes the ground-state configuration in ^{30}Ne. The transitional role of ^{28}Ne of having nearly degenerate $(sd)^n$ and $(sd)^{n-2}(pf)^2$ configurations has been noted [5], but the experimental ground-state binding energy for ^{28}Ne turns out to be in good agreement with all of the USD Hamiltonians.

For ^{26}F (shown in Fig. 15) the ground-state spin and energy are in agreement with theory but nothing is known about excited states. There are two levels below the neutron separation energy of 1 MeV. The 4^+ level should be isomeric and may β decay. The γ decay of the 2^+ level at 0.56 MeV (with USDB) to the ground state may correspond to the 0.66 MeV γ-ray decay reported in [77]. Levels for ^{26}O are shown in Fig. 16. The ground state of ^{26}O is bound to one-neutron decay by 0.80 (0.95) MeV with USDA (USDB), but it is unbound to two-neutron decay by 0.50 (0.35) MeV, in agreement with the experimental observation that it is unstable [67,68]. This unique situation for a dineutron decay would be interesting to observe experimentally. The predicted neutron-decay properties of $^{25-28}$O will be the subject of a separate paper.

For neutron-rich nuclei with $Z = 8$–10, the increase in the $d_{3/2}$ effective single-particle energy needed to improve the ground-state properties of nuclei with $N \geqslant 16$ is reflected in improvements in the spectra for excited states related to

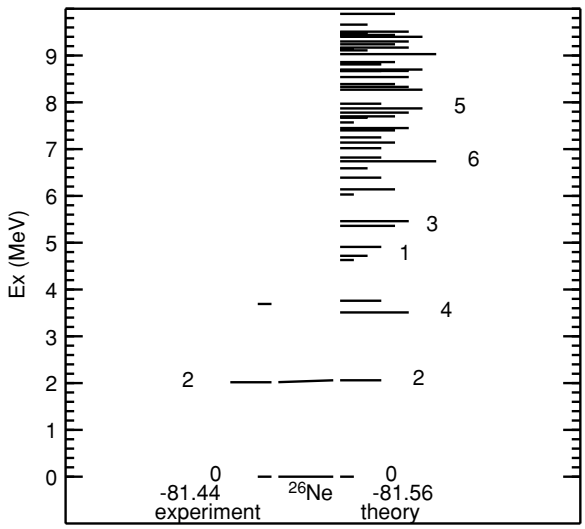

FIG. 14. Comparison of experimental and USDB theoretical levels for ^{26}Ne. See the text for details.

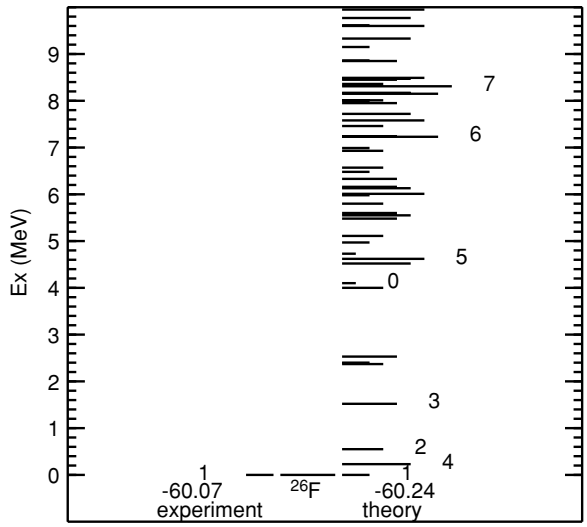

FIG. 15. Comparison of experimental and USDB theoretical levels for ^{26}F. See the text for details.

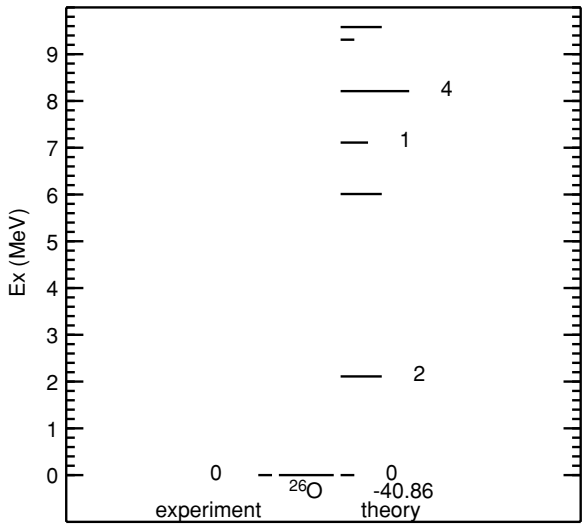

FIG. 16. Comparison of experimental and USDB theoretical levels for ^{26}O. See the text for details.

the $d_{3/2}$ orbit in nuclei with $14 \geqslant N \geqslant 16$. For example, the doublet of states near 2 MeV in ^{25}Ne is suggested to be on the order $3/2^{+}$-$5/2^{+}$ and is incorrect with the original USD [30], but is now corrected with USDA and USDB (see [71]). Excited states of ^{25}Ne were not included in the fit because the spin assignments are uncertain and because the recent experimental work [30] was published after the new fit was completed.

VI. SUMMARY AND CONCLUSIONS

The systematic application of USDA and USDB to other observables such as moments, electromagnetic decay, and β decay will be carried out over the foreseeable future. As a consequence we will gain a better understanding of the precision and limitation of this approach to nuclear structure. We should have more precise theoretical input for astrophysical applications such as those for electron-capture [78] and proton-capture cross sections [28] where experimental data cannot be obtained.

For this study we have used the renormalized G matrix from the Bonn-A potential as given in Table 20 of [33]. The results with Bonn-B and Bonn-C, also given in this table, show that there is some sensitivity to the NN interaction. We will explore which of the modern NN interactions and renormalization methods provide the best starting point for USD-type Hamiltonians.

From the introduction we repeat the reasons why the renormalized G-matrix sd-shell TBME may not be adequate: (i) The perturbation expansion may not be converged [34]; (ii) the oscillator basis used for matrix elements and energy denominators is an approximation; and (iii) real three-body forces are required as observed for ab initio calculations of light nuclei [35]. For (i) we may be able to apply the ab initio approaches used for lighter nuclei via a similarity transformation to evaluate an effective sd-shell Hamiltonian for $A = 18$. For (ii) we should explore the use of Hartree-Fock basis states in place of the harmonic oscillator for evaluation of the renormalized G matrix. For (iii) we need to find the contribution from realistic three-body forces to the effective two-body matrix elements for $A = 18$. The most important deviations to understand are the monopole interaction terms shown in Fig. 8.

Real and effective three-body interactions in principle require an explicit three-body interaction operator for three or more valence particles. However, the average effects of these three-body terms can be evaluated from an interaction calculated for two holes in the closed shell of ^{40}Ca (taking into account the three-body interaction explicitly). The USD Hamiltonians should be regarded as an average of the ab initio interactions for two particles and two holes. Eventually we may understand how much of the remaining 130- to 170-keV deviation between experiment and theory can be understood in terms of an explicit evaluation of the three-body Hamiltonian. With our updated database, new ideas can be readily incorporated into new versions of the USD-type Hamiltonians that are constrained by experimental data.

ACKNOWLEDGMENTS

We thank Dr. Honma for his computer program for the linear combination method fits. Support for this work was provided from U.S. National Science Foundation Grant Nos. PHY-0244453 and PHY-0555366 and by South African NRF ISL Grant GUN No. 2068517. This work is partly supported by the National Research Foundation of South Africa under Grant No. 2053790.

[1] B. H. Wildenthal, Prog. Part. Nucl. Phys. **11**, 5 (1984).
[2] B. A. Brown and B. H. Wildenthal, Annu. Rev. Nucl. Part. Sci. **38**, 29 (1988).
[3] E. K. Warburton and B. A. Brown, Phys. Rev. C **46**, 923 (1992).
[4] E. K. Warburton, J. A. Becker, and B. A. Brown, Phys. Rev. C **41**, 1147 (1990).
[5] Y. Utsuno, T. Otsuka, T. Mizusaki, and M. Honma, Phys. Rev. C **60**, 054315 (1999).
[6] S. Nummela *et al.*, Phys. Rev. C **63**, 044316 (2001).
[7] A. Heger *et al.*, Phys. Lett. **B606**, 258 (2005).
[8] K. Kaneko *et al.*, Phys. Rev. C **71**, 014319 (2005).
[9] P. Mason *et al.*, Phys. Rev. C **71**, 014316 (2005).
[10] M. Hasegawa and K. Kaneko, Nucl. Phys. **A748**, 393 (2005).
[11] A. Volya and V. Zelevinsky, Phys. Rev. Lett. **94**, 052501 (2005).
[12] V. Velazquez, J. G. Hirsch, A. Frank, J. Barea, and A. P. Zuker, Phys. Lett. **B613**, 134 (2005).
[13] Y. Parpottas *et al.*, Phys. Rev. C **72**, 025802 (2005).
[14] B. Davids *et al.*, Phys. Rev. Lett. **86**, 2750 (2001), and references therein.
[15] V. Tripathi *et al.*, Phys. Rev. Lett. **94**, 162501 (2005).
[16] W. Geithner *et al.*, Phys. Rev. C **71**, 064319 (2005).
[17] J. Y. Moon *et al.*, Nucl. Phys. **A758**, 158c (2005).
[18] R. G. T. Zegers *et al.*, Nucl. Phys. **A758**, 67c (2005).
[19] L. Weissman *et al.*, J. Phys. G **31**, 553 (2005).

[20] V. Guimaraes *et al*., Phys. Rev. C **61**, 064609 (2000).
[21] K. Kaneko and M. Hasegawa, Phys. Rev. C **72**, 031302(R) (2005).
[22] M. B. Tsang, J. Lee, and W. G. Lynch, Phys. Rev. Lett. **95**, 222501 (2005).
[23] F. Marechal *et al*., Phys. Rev. C **72**, 044314 (2005).
[24] M. Belleguic *et al*., Phys. Rev. C **72**, 054316 (2005).
[25] B. A. Brown and W. A. Richter, Phys. Rev. C **72**, 057301 (2005).
[26] V. Tripathi *et al*., Eur. Phys. J. A **25**, 101 (2005).
[27] A. F. Lisetskiy, A. Gelberg, and P. von Brentano, Eur. Phys. J. A **26**, 51 (2005).
[28] H. Schatz *et al*., Phys. Rev. C **72**, 065804 (2005).
[29] W. C. Haxton, K. M. Nollett, and K. M. Zurek, Phys. Rev. C **72**, 065501 (2005).
[30] S. W. Padgett *et al*., Phys. Rev. C **72**, 064330 (2005).
[31] J. Rotureau, J. Okolowicz, and M. Ploszajczak, Phys. Rev. Lett. **95**, 042503 (2005).
[32] M. Wiedeking *et al*., Phys. Rev. Lett. **92**, 132501 (2004).
[33] M. Hjorth-Jensen, T. T. S. Kuo, and E. Osnes, Phys. Rep. **261**, 125 (1995).
[34] B. R. Barrett and M. W. Kirson, Nucl. Phys. **A148**, 145 (1970).
[35] S. C. Pieper, V. R. Pandharipande, R. B. Wiringa, and J. Carlson, Phys. Rev. C **64**, 014001 (2001).
[36] A. P. Zuker, Phys. Rev. Lett. **90**, 042502 (2003).
[37] A. Arima, S. Cohen, R. D. Lawson, and M. H. MacFarlane, Nucl. Phys. **A108**, 94 (1968).
[38] W. Chung, Ph.D. thesis, Michigan State University, 1976.
[39] P. M. Endt, Nucl. Phys. **A633**, 1 (1998).
[40] P. M. Endt, Nucl. Phys. **A521**, 1 (1990); **A529**, 763 (1991) (Errata I); **A564**, 609 (1993) (Errata II).
[41] M. Stanoiu, *et al*., Phys. Rev. C **69**, 034312 (2004).
[42] D. Cortina-Gil *et al*., Phys. Rev. Lett. **93**, 062501 (2004).
[43] J. Pavan (private communication).
[44] Zs. Dombrádi (private communication).
[45] Z. Elekes *et al*., Phys. Lett. **B599**, 17 (2004).
[46] C. R. Hoffman *et al*., Phys. Rev. C **68**, 034304 (2003).
[47] M. W. Cooper *et al*., Phys. Rev. C **65**, 051302(R) (2002).
[48] I. Wiedenhöver, *et al*., Phys. Rev. Lett. **87**, 142502 (2001).
[49] J. Enders *et al*., Phys. Rev. C **65**, 034318 (2002).
[50] G. Audi, A. H. Wapstra, and C. Thibault, Nucl. Phys. **A729**, 337 (2003).
[51] H. Savajols *et al*., Eur. Phys. J. A **25**, Suppl. 1, 23(2005); W. Mittig (private communication, 2006).
[52] M. Honma, B. A. Brown, T. Mizusaki, and T. Otsuka, Nucl. Phys. **A704**, 134c (2002).
[53] P. R. Bevington and D. K. Robinson, *Data Reduction and Error Analysis*, 3rd ed. (McGraw-Hill, New York, 2003).
[54] M. H. Macfarlane, in *Two-Body Force in Nuclei*, edited by S. M. Austin and G. M. Crawley (Plenum Press, New York, 1972), p. 1.
[55] W. A. Richter, M. G. Van der Merwe, R. E. Julies, and B. A. Brown, Nucl. Phys. **A523**, 325 (1991).
[56] M. Honma, T. Otsuka, B. A. Brown, and T. Mizusaki, Phys. Rev. C **65**, 061301(R) (2002).
[57] A. F. Lisetskiy, B. A. Brown, M. Horoi, and H. Grawe, Phys. Rev. C **70**, 044314 (2004).
[58] B. A. Brown, A. Etchegoyen, N. S. Godwin, W. D. M. Rae, W. A. Richter, W. E. Ormand, E. K. Warburton, J. S. Winfield, L. Zhao, and C. H. Zimmerman, OXBASH for Windows, MSU-NSCL Report No. 1289.
[59] B. A. Brown, AIP Conference Proceedings **764**, 107 (2005).
[60] T. Otsuka, R. Fujimoto, Y. Utsuno, B. A. Brown, M. Honma, and T. Mizusaki, Phys. Rev. Lett. **87**, 082502 (2001).
[61] T. Otsuka, T. Suzuki, R. Fujimoto, H. Grawe, and Y. Akaishi, Phys. Rev. Lett. **95**, 232502 (2005).
[62] F. Ajzenberg-Selove, Nucl. Phys. **A281**, 1 (1977); S. E. Dardeen, S. Sen, H. R. Middleston, J. A. Aymar, and W. A. Yoh, *ibid*. **A208**, 77 (1973); M. D. Cooper, W. F. Hornyak, and P. G. Roos, *ibid.* **A218**, 249 (1974).
[63] P. Doll, G. J. Wagner, K. T. Knoepfle, and G. Mairle, Nucl. Phys. **A263**, 210 (1976).
[64] B. A. Brown and W. A. Richter, Phys. Rev. C **72**, 057301 (2005).
[65] M. Langevin *et al*., Phys. Lett. **B150**, 71 (1985).
[66] M. Thoennessen *et al*., Phys. Rev. C **68**, 044318 (2003).
[67] D. Guillemaud-Mueller *et al*., Phys. Rev. C **41**, 937 (1990).
[68] M. Fauerbach *et al*., Phys. Rev. C **53**, 647 (1996).
[69] H. Sakurai *et al*., Phys. Lett. **B448**, 180 (1999).
[70] O. Tarasov *et al*., Phys. Lett. **B409**, 64 (1997).
[71] http://www.nscl.msu.edu/∼brown/resouces/resources.html.
[72] R. D. Lawson, F. J. D. Serduke, and H. T. Fortune, Phys. Rev. C **14**, 1245 (1976).
[73] S. Lee *et al*., Phys. Rev. C **73**, 044321 (2006).
[74] L. Weissman *et al*., Phys. Rev. C **70**, 057306 (2004).
[75] B. H. Wildenthal, M. S. Curtin, and B. A. Brown, Phys. Rev. C **28**, 1343 (1983).
[76] B. A. Brown and B. H. Wildenthal, At. Data Nucl. Data Tables **33**, 347 (1985). The B(GT) as defined in the present work is related to the M(GT) of this reference by $B(\mathrm{GT}) = [M(\mathrm{GT})/1.251]^2/(2J_i + 1)$.
[77] M. A. Stanoiu, These, Universite de Caen/Basse-Normandie, 2003, p. 84.
[78] T. Kajino, E. Shiino, H. Toki, B. A. Brown, and B. H. Wildenthal, Nucl. Phys. **A480**, 175 (1988).